Available online at www.sciencedirect.com
ScienceDirect
Trans. Nonferrous Met. Soc. China 25(2015) 1367−1375
Transactions of Nonferrous Metals Society of China
www.tnmsc.cn

Microstructure and texture evolution of Al-7075 alloy processed by equal channel angular pressing

M. H. SHAERI[1], M. SHAERI[2], M. T. SALEHI[3], S. H. SEYYEDEIN[3], F. DJAVANROODI[4,5]

1. Department of Metallurgy and Materials Engineering, Engineering Faculty, Imam Khomeini International University, Qazvin 34149−16818, Iran;
2. Department of Materials Science and Engineering, Sharif University of Technology, Tehran, Iran;
3. Department of Metallurgy and Materials Engineering, Iran University of Science and Technology, Tehran, Iran;
4. Department of Mechanical Engineering, Iran University of Science and Technology, Tehran, Iran;
5. Department of Mechanical Engineering, Prince Mohammad Bin Fahd University, Al Khobar 31952, Saudi Arabia

Received 4 July 2014; accepted 25 October 2014

Abstract: Equal channel angular pressing is an effective technique to control the texture and microstructure of metals and alloys. Texture and microstructure of an Al-7075 alloy subjected to repetitive equal channel angular pressing through a 90° die were evaluated by X-ray diffractometer and orientation imaging microscopy. It is observed that processing through different routes leads to different types of textures, in both qualitative and quantitative senses. The texture calculation by Labotex software reveals that texture strengthens after the first pass and weakens by progressing ECAP process up to 4 passes. Microstructure investigations show that after 4 passes of equal channel angular pressing via routes B_C and A, very fine grains with average grain size of about 700 nm and 1 μm appear, respectively, and most of the grains evolve into arrays of high angle boundaries. The effects of covering the Al-7075 billets with copper tube on texture and microstructure were also studied.

Key words: equal channel angular pressing; crystallographic texture; aluminum alloy; ultra-fine grain

1 Introduction

Equal channel angular pressing (ECAP) or extrusion (ECAE) is known as the most promising technology among the potential severe plastic deformation (SPD) processing techniques, which can be applied to producing ultra-fine grained materials in bulk metallic alloys [1]. In equal channel angular pressing process, a billet is extruded repetitively through a die with two channels of equal cross section intersecting at an abrupt angle, Φ, and with a corner curvature angle, Ψ, [2,3]. Since the cross sectional shape of the billet remains nearly the same during the process, it is now well recognized as a promising method to enhance the strength of various metallic alloys through the occurrence of grain refinement in severe plastic deformation. In multi-pass ECAP, the evolution of crystallographic texture is quite complex due to the various strain path changes instigated by the prescribed processing route. The most common routes are termed A, C, B_A and B_C according to the rotation of the billet around the specimen's longitudinal axis between successive passes: A, no bar axis rotation; C, 180° rotation after each pass; B_A, clockwise 90° rotation after even numbered passes and counter clockwise 90° after odd numbered passes; and B_C, 90° rotation after each pass [3−8].

Investigation of texture evolution is essential to understand the mechanisms of plastic deformation and grain refinement during ECAP [9]. The large plastic deformation and strain-path changes involved in the process result in significant and complex changes of crystallographic texture [10]. In the literature, many studies have been conducted to evaluate the effects of material properties and processing variables on ECAP texture evolution [7−26]. For a given material, the texture development mainly depends on the die angle (Φ), processing route, number of passes (N) and initial texture [7,9,22−26]. On the characteristics of ECAP textures, most of the studies have shown that textures developed during ECAP deformation are often compared

Corresponding author: M. H. SHAERI; Tel: +98-2833901190; Fax: +98-2833780073; E-mail: shaeri@ENG.ikiu.ac.ir
DOI: 10.1016/S1003-6326(15)63735-9

with those after simple shear tests, such as torsion. This kind of comparison is a natural consequence of simple shear that has been accepted as the dominant deformation mode in ECAP [27−29].

The objective of the present work is to study the effect of equal channel angular pressing on texture and microstructure of Al-7075 alloy processed by routes A and B_C. For this purpose, conventional aluminum specimens and aluminum specimens covered with copper tube casing were analyzed by X-ray diffractometer (XRD) and orientation imaging microscopy (OIM) after 4 passes of ECAP, and then texture and microstructure of these specimens were compared.

2 Experimental

The experiments were conducted using Al-7075 alloy as the main ECAP material and commercial pure copper as covering tube. The chemical composition of Al-7075 alloy determined by the GNR Italy metallab−7580J spectrometer set is shown in Table 1. Extruded aluminum rods were machined into billets with diameter of 19.1 mm and length of 140 mm and then pressed through an ECAP solid die having a channel angle of Φ=90° and an outer curvature angle of Ψ=20°. The outer diameter and thickness of copper tube were 19.1 mm and 1 mm, respectively, so diameter of aluminum rod was decreased to 17.1 mm by lathing for specimens covered with copper tube. The copper tube and the rod were press fitted prior to the ECAP process. As reported in our previous work [30], covering the specimens with copper tube leads to a notable decrease in pressing load of ECAP process and a slight increase in homogenity and mechanical properties of ECAP processed specimens. The Al-7075 alloy and copper tubes were annealed at 415°C and 800 °C for 1 h followed by furnace cooling, respectively. Billets were pressed at room temperature for either 1 or 4 passes, equivalent to imposed strains of about 1 and 4, respectively [31], using processing routes A and B_C.

Table 1 Chemical composition of Al-7075 alloy (mass fraction, %)

Si	Fe	Cu	Mn	Mg	Cr	Zn	Ti	Al
0.07	0.09	1.50	0.04	2.65	0.21	5.70	0.02	Bal.

Measurements of crystallographic texture were performed employing a RIGAKU, D/MAX−2500 X-ray diffractometer (Cu K_α radiation, λ=1.5406 Å) on the flow or *Y* plane equivalent to the side plane at the point of exit from the ECAP die (Fig. 1[32]). The measurements were taken at approximately the mid-point on each longitudinal section by preparing a flat surface through mechanical polishing and grinding. The textures recorded over an area having dimensions of 19 mm × 19 mm. X-ray pole figures (PF) measurements were carried out using Schulz back reflection method. The Labotex 2.1 software was used to process the raw data, calculate the orientation distribution function (ODF) from three partial pole figures (111), (200) and (220), and calculate volume fraction of the texture components. After definition of the main ideal ECAP texture components by the Euler angles or Miller indices in the Labotex software, the volume fractions of the texture components were measured by integration method. The volume fractions were computed by integrating the ODF within a 10° distance in Euler space from the ideal component orientation. It might result in some limited overlapping of the volume fractions of neighboring components, nevertheless, the relative strengths of the components were well represented by this technique.

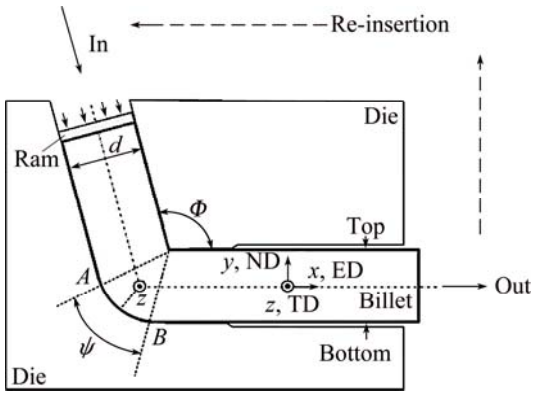

Fig. 1 ECAP die geometry and coordinate system employed

The microstructural examination was carried out using a Quanta 3D FEI field emission scanning electron microscope (FE-SEM) with electron back scatter diffractometer (EBSD) attachment at an accelerating voltage of 15 kV and a beam current of 10 nA. The orientation image microscopy (OIM) images were obtained on the area of 80 μm ×150 μm with the step size of 500 nm for annealed specimen, whereas for ECAP processed specimens the OIM images were obtained on the area of 7 μm × 12 μm with the step size of 50 nm. The results were analyzed using the TSL software. The collected data were subjected to a clean-up procedure consisting of: 1) grain dilation with grain tolerance angle of 5° and a minimum grain size of 2 pixels; 2) grain confidence index (CI) standardization with grain tolerance angle of 5° and minimum grain size equal to 2 pixels; 3) neighbor orientation correlation (level 4) with a minimum CI of 0.02. For specimen preparation, the surface of cross-section (*X*-plane in Fig. 1) was first mechanically ground up to 4000-grit SiC paper, then electropolishing was employed in a 30% nitric acid and

70% methanol solution. The electropolishing was carried out with a DC voltage of 15 V at −25 °C for 10 s.

3 Results and discussion

3.1 Initial texture and microstructure

Figure 2 shows optical image (etchant: Weck's color reagent [33]) and EBSD micrograph of the material before ECAP. As can be seen, the microstructure of starting material consists of grains with grain size in the range of 10−80 μm, and sub-grains with grain size less than 5 μm. EBSD orientation color maps and (200) and (111) pole figures of the starting material are shown in Fig. 3 in the laboratory reference system projected in the *X* plane, which is initially perpendicular to the specimen longitudinal axis. The grain colors are determined by the orientation of each grain as depicted in the unit triangle. As shown in Fig. 3, the texture of the starting material consists of strong ⟨100⟩ fiber together with a weak ⟨111⟩ fiber, with the fiber axis parallel to the billet longitudinal axis (*x* direction). The grains with ⟨100⟩ and ⟨111⟩ fiber textures are shown with red and blue colors in Fig. 3, respectively. Texture calculations by Labotex software demonstrate that about 68% of starting material texture is ⟨100⟩ fiber and about 20% is ⟨111⟩ fiber.

3.2 Texture evolution of ECAP processed specimens

The experimental (111) pole figures (PF) of ECAP processed materials for 1 pass and 4 passes by route A and B_C are shown in Fig. 4. As the ECAP deformation is near simple shear in the intersection plane of the two channels, the ideal ECAP texture components are the same as those known already for simple shear; they are just rotated by 45° with respect to the ECAP reference system [8,34]. In order to evaluate the textures developed during ECAP, the symbols marked in the key (111) PF (Fig. 4(b)) represent the ideal ECAP orientations for FCC metals [10]. To aid characterization of ECAP textures, Table 2 provides a summary of the Euler angles and Miller indices for the main ideal texture components of ECAP processed FCC materials for Φ=90°, based on the calculations by LI et al [10] and CHOWDHURY et al [35]. As shown in Fig. 4, monoclinic symmetry can be well identified in the pole figures of 1 pass ECAP processed specimen and 4 passes ECAP processed specimen by route A, while it is absent in 4 passes ECAP processed specimen by route B_C. The monoclinic symmetry refers to invariance about 180° rotation around TD axis of the die. Due to the monoclinic symmetry of the initial texture, the monoclinic symmetry remains after the first ECAP pass. Sample rotation around any

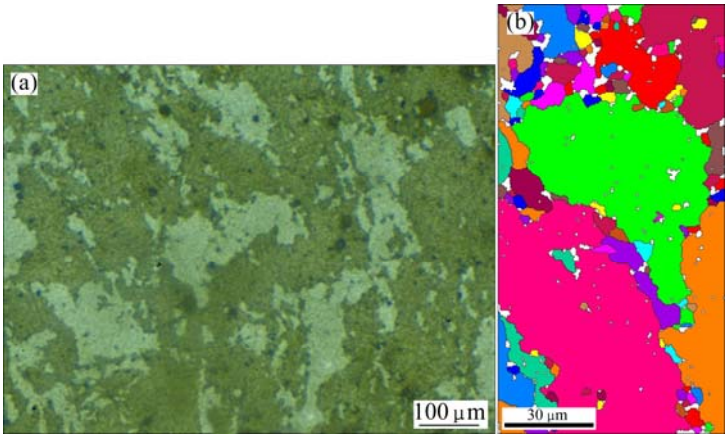

Fig. 2 Optical image (etchant: Weck's color reagent) (a) and EBSD micrograph (grain color map) (b) of starting material

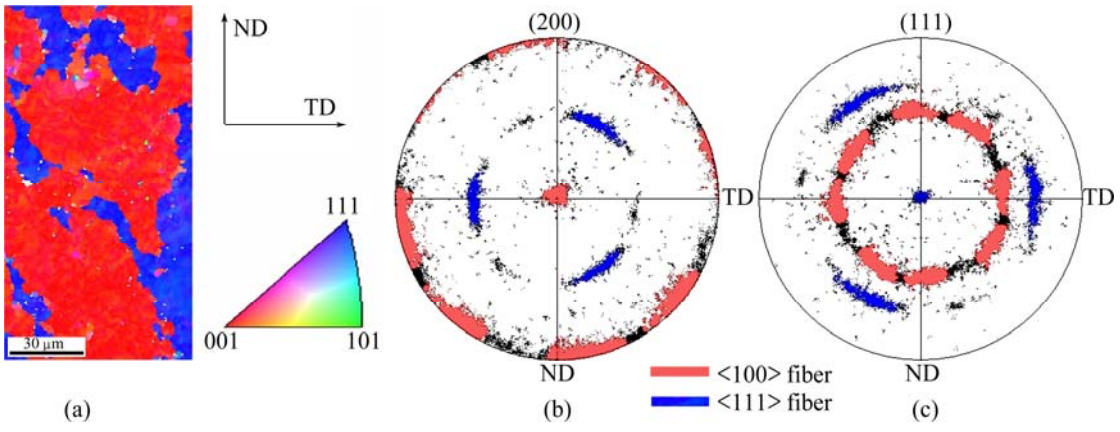

Fig. 3 EBSD orientation color map (IPF map) (a) and (200) (b) and (111) (c) pole figures of starting material

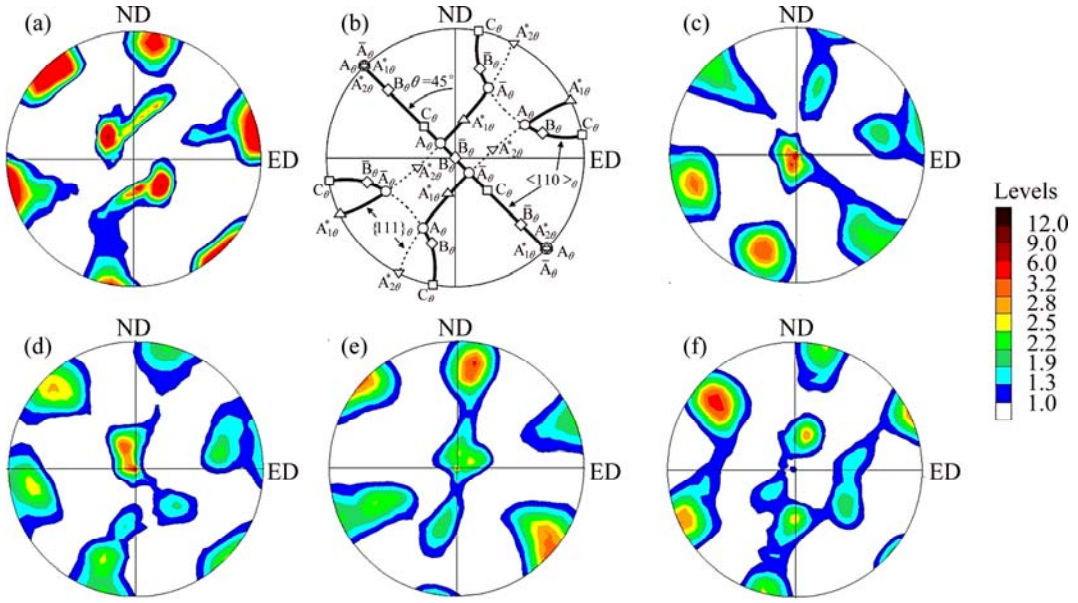

Fig. 4 Experimental (111) pole figures of ECAP processed materials for 1 pass (a), ideal ECAP orientations for FCC metals (b), 4 passes in route A (c), 4 passes in route A (d) (specimen with copper tube casing), 4 passes in route B_C (e) and 4 passes in route B_C (f) (specimen with copper tube casing)

Table 2 Ideal ECAP orientations for FCC materials and Φ=90° die [11]

Notation	Euler angle/(°)			Miller index		
	φ_1	Φ	φ_2	ND	ED	TD
$A^*_{1\theta}$	80.26/260.26	45	0	[8 1 $\bar{1}$]	[1 $\bar{4}$ 4]	[0 1 1]
$A^*_{2\theta}$	9.74/189.74	45	0	[1 $\bar{4}$ 4]	[8 1 $\bar{1}$]	[0 1 1]
A_θ	45	35.26	45	[9 1 4]	[1 11 $\bar{5}$]	[$\bar{1}$ 1 2]
$\bar{A}_\theta$	225	35.26	45	[$\bar{1}$ $\bar{11}$ 5]	[$\bar{9}$ $\bar{1}$ $\bar{4}$]	[$\bar{1}$ 1 2]
B_θ	45/165/285	54.74	45	[15 4 11]	[7 26 $\bar{19}$]	[$\bar{1}$ 1 1]
$\bar{B}_\theta$	105/225/345	54.74	45	[$\bar{7}$ $\bar{26}$ 19]	[$\bar{15}$ $\bar{4}$ $\bar{11}$]	[$\bar{1}$ 1 1]
C_θ	135/315	90	0	[3 3 4]	[2 2 $\bar{3}$]	[$\bar{1}$ 1 0]

other axis except TD leads to the loss of monoclinic symmetry, so, monoclinic symmetry is maintained in route A for many passes, while it is lost in route B_C after the first pass as a result of rotation around ED axis [11,32].

A detailed analysis of the textures was carried out by using the ODF representation. The advantage of displaying the ECAP textures in orientation space in contrast to pole figures is that the ideal orientations appear separately, without overlapping [36]. Figure 5 represents the φ_2=0° and φ_2=45° sections of the ODFs, which are sufficient if one is only interested in the ideal components of ECAP textures. The ideal ECAP texture components are presented in a key ODF (Fig. 5(f)). The examination of the ODFs reveals that the maximum intensity $f(g)_{max}$ increases significantly by the first pass of ECAP process, and decreases notably by progressing ECAP process up to 4 passes.

Texture strength is often measured by a texture index. The texture index, T, characterizes the overall intensity of a texture and is defined as follows: [37]

$$T = \int_{\text{Euler space}} [f(g)]^2 \mathrm{d}g \quad (1)$$

where g is the orientation defined by the Euler angle and $f(g)$ is the ODF intensity at g. Meanwhile, as shown by the T values (Table 3), texture strength of 1 pass ECAP processed specimen is about 2 times higher that of starting material, while by increasing ECAP passes, texture strength decreases more than 4 times [18]. Another important finding from T values is a slight decrease in texture strength of ECAP processed specimens covered with copper tube compared with those of specimens without copper tube, so it can be concluded that, by covering the specimens with copper tube, the crystallographic texture weakens slightly. To provide an appropriate quantitative comparison between texture components of ECAP processed specimens

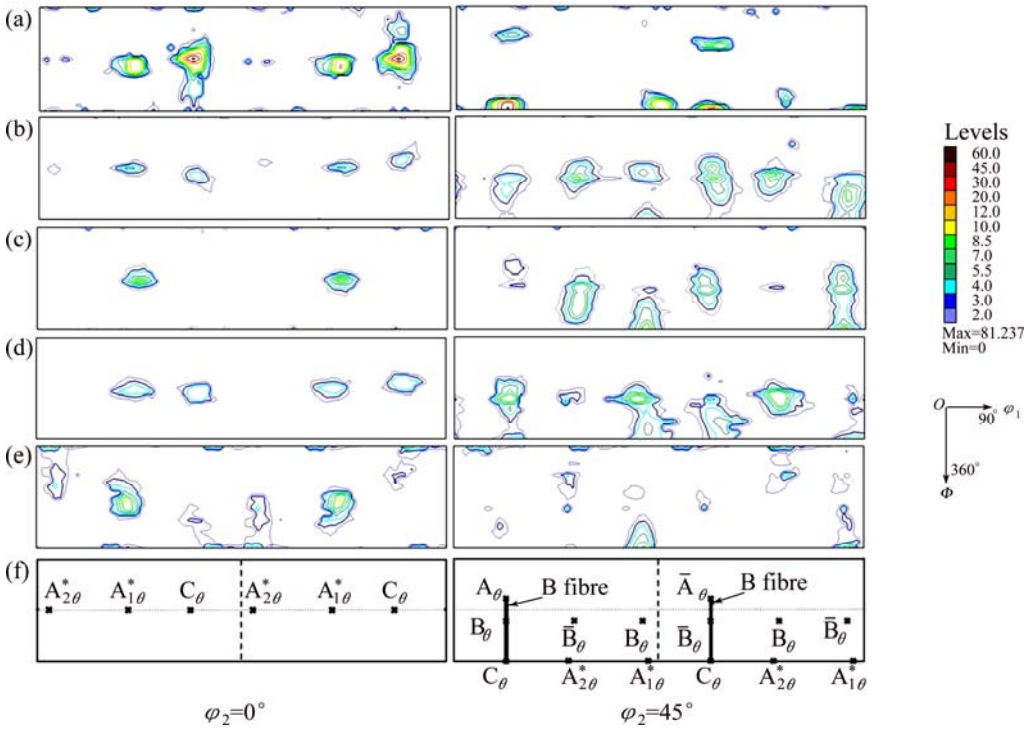

Fig. 5 ODF sections of ECAP processed materials for 1 pass (a), 4 passes in route A (b), 4 passes in route B_C (c), 4 passes in route A (d) (specimen with copper tube casing), 4 passes in route B_C (e) (specimen with copper tube casing) and ideal ECAP orientations for FCC metals (f)

Table 3 Volume fractions (%) of ideal ECAP texture components and texture indexes of starting material and EACP processed specimens

Texture component	4 passes ECAP				1 pass ECAP	Starting material
	Route B_C		Route A			
	With Cu tube	Without Cu tube	With Cu tube	Without Cu tube		
⟨100⟩ fiber	−	−	−	−	−	68
⟨111⟩ fiber	−	−	−	−	−	20
A_θ	1.1	1.2	1.8	1.5	2.4	−
$\bar{A}_\theta$	0.3	2.4	1.3	2.1	2.9	−
B_θ	0.7	1.4	3.8	3.6	0.1	−
$\bar{B}_\theta$	1.5	3.2	2.4	4.4	0.1	−
$A^*_{2\theta}$	1.2	0.9	0.7	0.9	1.3	−
$A^*_{1\theta}$	4.9	4.2	2.9	2.4	5.8	−
C_θ	0.8	0.7	2.4	1.8	14.5	−
Texture index	2.1	2.3	2.1	2.4	10.3	4.7

in different conditions, volume fractions of ideal ECAP texture components were calculated by Labotex software (Table 3).

1) N=1

As can be seen in Fig. 5(a) as well as Table 3, in the first pass, C_θ is the strongest component, $A^*_{1\theta}$ is approximately strong, $A_\theta/\bar{A}_\theta$ components are moderate, $A^*_{2\theta}$ is weak and $B_\theta/\bar{B}_\theta$ are absent. Since, the intensity of A_θ and $\bar{A}_\theta$ as well as B_θ and $\bar{B}_\theta$ components are approximately equal, it is obvious that the monoclinic symmetry is present in 1 pass ECAP processed specimen [11]. It is important to mention that when the initial texture is strong, the textures of the first few passes are relevant to the initial texture [18,24,32,36]. So, it can be concluded that, the high intensity of $A^*_{1\theta}$ and specially C_θ components compared with other ECAP ideal components, may be related to initial strong ⟨100⟩ and ⟨111⟩ fiber textures. Figure 6 shows that the $A^*_{1\theta}$ and specially C_θ components have good conformity with pole figure of initial texture and the conformity of the other

texture components with initial texture is less. So, it is obvious that the initial texture has considerable effect on the texture of the first pass of ECAP.

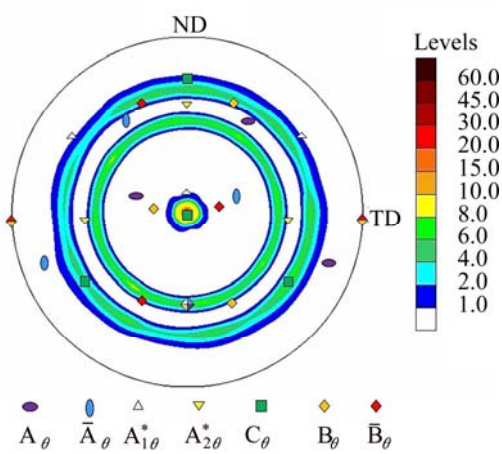

Fig. 6 Location of ideal ECAP texture components on ⟨111⟩ pole figure of initial specimen (ED plane)

2) N=4 (Route A)

As shown in Fig. 5(b) and Table 3, with the increase of pass number through route A, the $B_\theta/\bar{B}_\theta$ components become stronger and the C_θ component becomes weaker. $B_\theta/\bar{B}_\theta$ components are the strongest in 4 passes ECAP processed by route A, and $A^*_{2\theta}$ is the weakest component. The other components (C_θ, $A^*_{1\theta}$, $A_\theta/\bar{A}_\theta$) have moderate intensities [11]. In fact, the tendency of strengthening $B_\theta/\bar{B}_\theta$ with pass number through route A can also be seen in experimental textures presented by WERENSKIOLD and ROVEN [20] in AA6182 alloy, SUWAS et al [16] in silver, GHOLINIA et al [13] in pure aluminum and LI et al [19] in pure copper. ARRUFFAT-MASSION et al [12,34,36] stated that the reason of $B_\theta/\bar{B}_\theta$ components strengthening with N lies in −90° rotation of ECAP specimen around the TD axis between each pass, and symmetrical location of $B_\theta/\bar{B}_\theta$ components at every 60° in orientation space. It should be noted that strengthening of $B_\theta/\bar{B}_\theta$ with pass number depending on various factors such as material properties, initial texture, grain refinement process and twinning activity [12,34,36].

Similar to 1 pass ECAP processed specimens, the intensity of A_θ and $\bar{A}_\theta$ as well as B_θ and $\bar{B}_\theta$ components are approximately equal, so as discussed previously, it can be deduced that, monoclinic symmetry of the texture maintained in specimens ECAP processed for 4 passes by route A. Comparing volume fraction of texture components (Table 3) and corresponding ODF sections (Figs. 5(b) and (d)) of specimens ECAP processed with copper tube casing and without copper tube casing by route A, it reveals that all texture components intensities except C_θ and $A^*_{1\theta}$ decrease slightly by covering the Al-7075 billets with copper tube. Investigation of $A_\theta/\bar{A}_\theta$ and $B_\theta/\bar{B}_\theta$ components demonstrates that monoclinic symmetry of ECAP processed specimens with copper tube is less than those ECAP processed without copper tube.

3) N=4 (route B_C)

After 4 passes of ECAP by route B_C, $A^*_{1\theta}$ component is the strongest and C_θ component disappears. A_θ and B_θ components are weak and $\bar{A}_\theta$ and $\bar{B}_\theta$ components are moderate, so it can be concluded that the monoclinic symmetry is absent in route B_C, because the intensities of A_θ and $\bar{A}_\theta$ as well as B_θ and $\bar{B}_\theta$ components are different (Fig. 5(c) and Table 3) [11]. Due to the complexity in the deformation imposed by route B_C, textures in this route are difficult to be characterized. The reason of this complexity is that the specimen is rotated between passes around TD and ED axes [7,32]. Present study confirms the studies of LI et al [7,18] who reported that the highest orientation density is found near $A^*_{1\theta}$ in 4 passes ECAP processed specimens by route B_C. Based on the results displayed in Figs. 5(c) and (e) and Table 3, it can be deduced that, covering the Al-7075 billets with copper tube leads to a notable reduction in volume fraction of $\bar{A}_\theta$, B_θ and $\bar{B}_\theta$ components and a slight increment in volume fraction of $A^*_{1\theta}$ component.

3.3 Microstructure of ECAP processed specimens

Figures 7 and 8 show typical EBSD maps obtained from the center portion of the samples subjected to 4 passes of ECAP on the section perpendicular to the pressing axis (x-plane). Figure 7 indicates the crystallographic orientations of the grains perpendicular to the pressing direction, where the grain colors are determined by the orientation of each grain as depicted in the unit triangle in Fig. 3(a). Figure 8 illustrates the corresponding grain boundary maps in which the high angle grain boundaries with misorientation angle above 15° are shown as black lines, while boundaries between 5° and 15° and between 2° and 5° are shown as green and red lines, respectively.

In general, grains with misorientations greater than 15° are considered as effective grains, and area fraction method were used for average grain size calculation by TSL software. The average grain size is calculated by following equation:

$$\bar{v}=\frac{\sum_{i=1}^{n}A_i v_i}{\sum_{i=1}^{n}A_i} \tag{2}$$

where n is the total number of grains, v_i is the grain size for grain i and A_i is the area of grain i.

According to the EBSD experiments, the average grain size of the initial microstructure is observed to be about 40 μm. After 4 passes of ECAP by routes B_C and

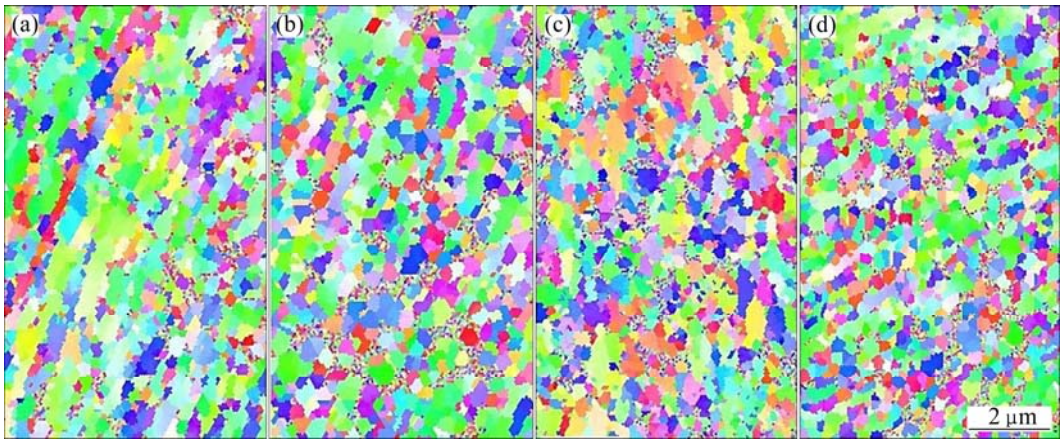

Fig. 7 EBSD orientation color maps (IPF map) of ECAP processed materials for 4 passes in route A (a), 4 passes in route A (b) (specimen with copper tube casing), 4 passes in route B_C (c) and 4 passes in route B_C (d) (specimen with copper tube casing)

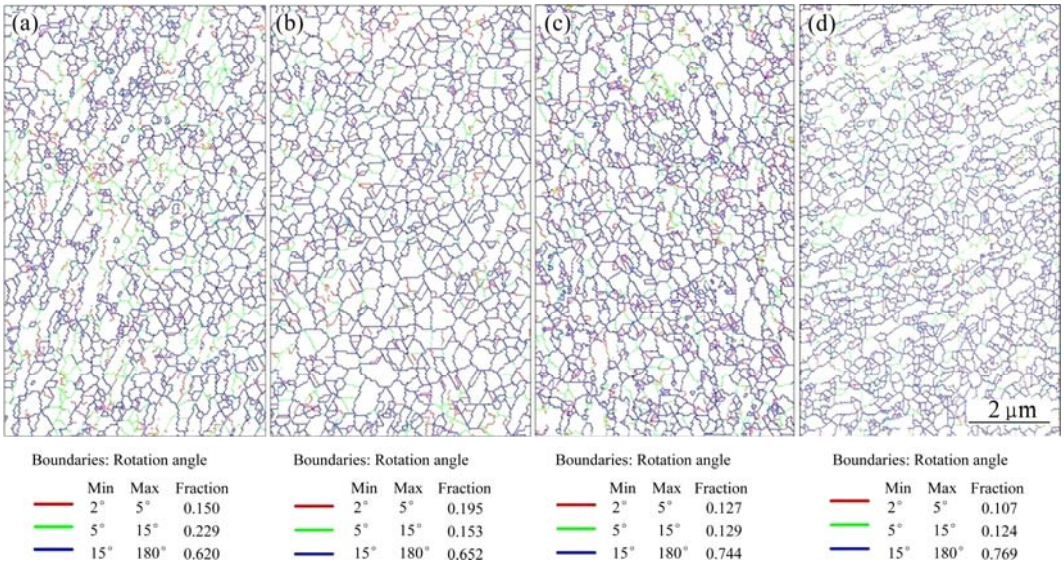

Fig. 8 EBSD grain boundary maps of ECAP processed materials for 4 passes in route A (a), 4 passes in route A (b) (specimen with copper tube casing), 4 passes in route B_C (c) and 4 passes in route B_C (d) (specimen with copper tube casing)

A, the grain size reduces to about 600 nm and 900 nm, respectively. As shown in Figs. 7(a) and (c), the specimen subjected to ECAP process by route B_C demonstrates relatively equiaxed grains with irregular orientations, while the specimen subjected to ECAP process by route A demonstrates somewhat elongated grains with a crystal orientation that tended to be tilted in the shear direction imposed by ECAP. Comparing the grains aspect ratio of the specimen ECAP processed by route A (1.64) and that of specimen ECAP processed by route B_C (1.44) also reveals that the specimen ECAP processed by route B_C has more equiaxed grains. Figure 8(c) shows that when pressing the specimen 4 passes by route B_C, the microstructure mainly consists of high angle grain boundaries (about 75%), while 25% of boundaries in initial material were high angle boundaries. Microstructural comparison between 4 passes ECAP processed specimens by routes A and B_C (Figs. 8(a) and (c)) reveals that the volume fraction of high angle grain boundaries in route A specimens is 15% less than that in route B_C specimens. Based on the results obtained, it can be concluded that, route B_C appears preferable to route A for obtaining equiaxed grains with high angle boundaries, during refining grains through ECAP. The reason lies in different shear systems in routes A and B_C. Route B_C has two shear directions lie on planes which intersect at 120°, while route A has two shear planes intersecting at 90° [38−41]. Comparing the EBSD results in current investigation with the TEM results in our previous work [11] reveals that the grain size, fraction of high angle grain boundaries and grains equiaxiality measured by EBSD are reasonably consistent with the data measured by TEM.

Figures 7(b), (d) and Figs. 8(b), (d) show that

covering the specimens with copper tube do not have considerable effects on microstructure; however, these results demonstrate that covering the specimens with copper tube may lead to a slight decline in grain size, and also a slight increment in grains homogeneity. The grain size of ECAP processed specimens covered with copper tube is about 200 nm less than that of specimens ECAP processed without copper tube. By covering the specimens with copper tube, volume fraction of high angle grain boundaries increases about 3% and also grains become more equiaxed. By covering the specimens with copper tube, the grains aspect ratios of the specimens ECAP processed by routes A and B_C decrease from 1.64 to 1.56 and 1.44 to 1.38, respectively. This conclusion has a good conformity with our previous work, which reported that by covering the sample with copper tube, mechanical properties and homogeneity increase [30].

4 Conclusions

1) The textures of Al-7075 with an initially strong duplex fiber texture that develop during ECAP process depend strongly on the ECAP route and pass number. Texture strength of starting material, 1 pass and 4 passes ECAP processed specimens are 4.7, 10.3 and 2, respectively. So, it can be concluded that, after the first pass, texture strength increases, and then by increasing pass number up to 4 passes, texture strength decreases significantly.

2) According to the strong initial texture of starting material, the texture of the first pass is relevant to initial texture, but by increasing pass number, this dependency disappears. In 1 pass ECAP processed specimens, C_θ is the strongest component, while after 4 passes, $B_\theta/\overline{B}_\theta$ and $A^*_{1\theta}$ are the strongest components in routes A and B_C, respectively.

3) The initial average grain size of about 40 μm was refined down to about 600 nm and 900 nm after 4 passes by routes A and B_C, respectively. The route A specimen showed an inhomogeneous microstructure with elongated grains compared with the route B_C specimen.

4) EBSD analysis showed that after 4 passes of ECAP, the volume fraction of high angle grain boundaries increases significantly (about 3 times). On the other hand, route B_C is more beneficial for obtaining high angle grain boundaries.

5) Texture and microstructure investigations show that by covering the specimens with copper tube, volume fraction of the most of the texture components, grain size and microstructure inhomogeneity slightly decrease.

References

[1] VALIEV R Z, LANGDON T G. Principles of equal-channel angular pressing as a processing tool for grain refinement [J]. Prog Mater Sci, 2006, 51: 881−981.

[2] XU C, LANGDON T G. Influence of a round corner die on flow homogeneity in ECA pressing [J]. Scr Mater, 2003, 48: 1−4.

[3] XU C, LANGDON T G. The development of hardness homogeneity in aluminum and an aluminum alloy processed by ECAP [J]. J Mater Sci, 2007, 42: 1542−1550.

[4] ZHANG Jing, ZHANG Ke-shi, WU Hwai-chung, YU Mei-hua. Experimental and numerical investigation on pure aluminum by ECAP [J]. Transactions of Nonferrous Metals Society of China, 2009, 19: 1303−1311.

[5] JIANG Da-ming, NING Jiang-li, SUN Jiang-feng, HU Zhi-min, HOU Yi. Annealing behavior of Al−Mg−Mn alloy processed by ECAP at elevated temperature [J]. Transactions of Nonferrous Metals Society of China, 2008, 18(2): 248−254.

[6] SHAERI M H, SALEHI M T, SEYYEDEIN S H, ABUTALEBI M R, PARK J K. Microstructure and mechanical properties of Al-7075 alloy processed by equal channel angular pressing combined with aging treatment [J]. J Mater Des, 2014, 57: 250−257.

[7] LI S, BEYERLEIN I J, ALEXANDER D J, VOGEL S C. Texture evolution during multi-pass equal channel angular extrusion of copper: Neutron diffraction characterization and polycrystal modeling [J]. Acta Mater, 2005, 53: 2111−2125.

[8] SUWAS S, ARRUFFAT-MASSION R, TÓTH L S, FUNDENBERGER J J, BEAUSIR B. Evolution of texture during equal channel angular extrusion of commercially pure aluminum: Experiments and simulations [J]. Mater Sci Eng A, 2009, 520: 134−146.

[9] LI S, BEYERLEIN I J, ALEXANDER D J. Characterization of deformation textures in pure copper processed by equal channel angular extrusion via route A [J]. Mater Sci Eng A, 2006, 431: 339−345.

[10] LI S, BEYERLEIN I J, BOURKE M A M. Texture formation during equal channel angular extrusion of fcc and bcc materials: Comparison with simple shear [J]. Mater Sci Eng A, 2005, 394: 66−77.

[11] SHAERI M H, SALEHI M T, SEYYEDEIN S H, ABUTALEBI M R, PARK J K. Characterization of microstructure and deformation texture during equal channel angular pressing of Al−Zn−Mg−Cu alloy [J]. J Alloy Comp, 2013, 579: 350−357.

[12] ARRUFFAT-MASSION R, SUWAS S, TÓTH L S, SKROTZKI W, FUNDENBERGER J J, EBERHARDT A. Experiments and modeling of ECAE textures of fcc polycrystals [J]. Mater Sci Forum 2005, 495−497: 839−844.

[13] GHOLINIA A, BATE P, PRANGNELL P B. Modelling texture development during equal channel angular extrusion of aluminum [J]. Acta Mater, 2002, 50: 2121−2136.

[14] WU Bao-lin, HUANG Zhen-wei, ZHANG Yu-dong, BAO Lei, ESLING C. Deformed texture of copper processed by equal channel angular pressing via different angle routes [J]. Transactions of Nonferrous Metals Society of China, 2007, 17(3): 479−485.

[15] ZHANG Fan, ZHANG Ke-xiang, TAN Cheng-wen, YU Xiao-dong, MA Hong-lei, WANG Fu-chi, CAI Hog-nian. Microstructure and mechanical properties of Mg−Gd−Y−Zr alloy processed by equal channel angular pressing [J]. Transactions of Nonferrous Metals Society of China, 2011, 21(10): 2140−2146.

[16] SUWAS S, TÓTH L S, FUNDENBERGER J J, EBERHARDT A, SKROTZKI W. Evolution of crystallographic texture during equal channel angular extrusion of silver [J]. Scripta Mater, 2003, 49: 1203−1208.

[17] SALIMYANFARD F, TOROGHINEJAD M R, ASHRAFIZADEH F, HOSEINI M, SZPUNAR J A. Investigation of texture and mechanical properties of copper processed by new route of equal channel angular pressing [J]. J Mater Des, 2013, 44: 374−381.

[18] LI S, BEYERLEIN I J, ALEXANDER D J, VOGEL S C. Texture evolution during equal channel angular extrusion: Effect of initial

texture from experiment and simulation [J]. Scripta Mater, 2005, 52: 1099−1104.
[19] LI S, BEYERLEIN I J, NECKER C T, ALEXANDER D J, BOURKE M. Heterogeneity of deformation texture in equal channel angular extrusion of copper [J]. Acta Mater, 2004, 52: 4859−4875.
[20] WERENSKIOLD J C, ROVEN H J. Microstructure and texture evolution during ECAP of an AlMgSi alloy: Observations, mechanisms and modeling [J]. Mater Sci Eng A, 2005, 410−411: 174−177.
[21] ETTER A L, BAUDIN T, REY C, PENELLE R. Microstructural and textural characterization of copper processed by ECAE [J]. Mater Character, 2006; 56: 19−25.
[22] HAOUAOUI M, HARTWIG K T, PAYZANT E A. Effect of strain path on texture and annealing microstructure development in bulk pure copper processed by simple shear [J]. Acta Mater, 2005, 53: 801−810.
[23] LI S, GAZDER A A, BEYERLEIN I J, PERELOMA E V, DAVIES C H J. Effect of processing route on microstructure and texture development in equal channel angular extrusion of interstitial-free steel [J]. Acta Mater, 2006, 54: 1087−1100.
[24] FERRASSE S, SEGAL V M, KALIDINDI S R, ALFORD F. Texture evolution during equal channel angular extrusion (Part I): Effect of route, number of passes and initial texture [J]. Mater Sci Eng A, 2004, 368: 28−40.
[25] LI S, BEYERLEIN I J. Modelling texture evolution in equal channel angular extrusion of bcc materials: Effects of processing route and initial texture [J]. Model Simul Mater Sci Eng, 2005, 13: 509−530.
[26] BAIK S C, ESTRIN Y, HELLMIG R J, JEONG H T, BROKMEIER H G, KIM H S. Modeling of texture evolution of copper under equal channel angular pressing [J]. Z Metallkd, 2003, 94: 1189−1198.
[27] SEGAL V M. Equal channel angular extrusion: From macromechanics to structure formation [J]. Mater Sci Eng A, 1999, 271: 322−333.
[28] KIM H S. Evaluation of strain rate during equal channel angular pressing [J]. J Mater Res, 2002, 17: 172−179.
[29] LI S, BOURKE M A M, BEYERLEIN I J, ALEXANDER D J, CLAUSEN B. Finite element analysis of the plastic deformation zone and working load in equal channel angular extrusion [J]. Mater Sci Eng A, 2004, 382: 217−236.
[30] SHAERI M H, DJAVANROODI F, AHMADI S, SEDIGHI M, SALEHI M T, SEYYEDEIN S H. The effect of copper tube casing on homogeneity and mechanical properties of Al 7075 alloy processed by the equal channel angular pressing [J]. J Strain Analysis Eng Des, 2013, 48: 512−521.
[31] IWAHASHI Y, WANG J, HORITA Z, NEMOTO M, LANGDON T G. Principle of equal-channel angular pressing for the processing of ultra-fine grained materials [J]. Scripta Mater, 1996, 35: 143−146.
[32] BEYERLEIN I J, TÓTH L S. Texture evolution in equal-channel angular extrusion [J]. Prog Mater Sci, 2009, 54: 427−510.
[33] WECK E, LEISTNER E. Metallographic instructions for colour etching by immersion [M]. Part III. Germany: DVS Verlay GmbH-Düsseldorf, 1986.
[34] TÓTH L S, ARRUFFAT-MASSION R, GERMAIN L, BAIK S C, SUWAS S. Analysis of texture evolution in equal channel angular extrusion of copper using a new flow field [J]. Acta Mater, 2004, 52: 1885−1898.
[35] CHOWDHURY S G, XU C, LANGDON T G. Texture evolution in an aluminum alloy processed by ECAP with concurrent precipitate fragmentation [J]. Mater Sci Eng A, 2008, 473: 219−225.
[36] SUWAS S, ARRUFFAT-MASSION R, TÓTH L S, FUNDENBERGER J J, EBERHARDT A, SKROTZKI W. Evolution of crystallographic texture during equal channel angular extrusion of copper: The role of material variable [J]. Metall Mater Trans A, 2006, 37: 739−753.
[37] BUNGE H J. Texture analysis in materials science [M]. London: Butterworth and Co, 1982.
[38] IWAHASHI Y, FURUKAWA M, HORITA Z, NEMOTO M, LANGDON T G. Microstructural characteristics of ultrafine-grained aluminum produced using equal-channel angular pressing [J]. Metall Mater Trans A, 1998, 29: 2245−2252.
[39] KIM Y G, KO Y G, SHIN D H, LEE S. Effect of equal-channel angular pressing routes on high-strain-rate deformation behavior of ultra-fine-grained aluminum alloy [J]. Acta Mater, 2010, 58: 2545−2554.
[40] IWAHASHI Y, HORITA Z, NEMOTO M, LANGDON T G. The process of grain refinement in equal-channel angular pressing [J]. Acta Mater, 1998, 46: 3317−3331.
[41] VENKATACHALAM P, KUMAR S R, RAVISANKAR B, PAUL V T, VIJAYALAKSHMI M. Effect of processing routes on microstructure and mechanical properties of 2014 Al alloy processed by equal channel angular pressing [J]. Transactions of Nonferrous Metals Society of China, 2010, 20: 1822−1828.

等径角挤压 7075 铝合金的显微组织和织构演变

M. H. SHAERI[1], M. SHAERI[2], M. T. SALEHI[3], S. H. SEYYEDEIN[3], F. DJAVANROODI[4,5]

1. Department of Metallurgy and Materials Engineering, Engineering Faculty, Imam Khomeini International University, Qazvin 34149−16818, Iran;
2. Department of Materials Science and Engineering, Sharif University of Technology, Tehran, Iran;
3. Department of Metallurgy and Materials Engineering, Iran University of Science and Technology, Tehran, Iran;
4. Department of Mechanical Engineering, Iran University of Science and Technology, Tehran, Iran;
5. Department of Mechanical Engineering, Prince Mohammad Bin Fahd University, Al Khobar 31952, Saudi Arabia

摘　要：等径角挤压是一种有效的控制金属和合金显微组织和织构的技术。采用 X 射线衍射仪和取向成像显微镜评价通过 90°模具反复等径角挤压 7075 铝合金的显微组织和织构。定性和定量分析结果表明，不同的路径会产生不同的织构类型。利用 Labotex 软件计算的织构表明，经第 1 道次等径角挤压后合金织构增强，而经第 4 道次挤压后合金织构减弱。显微组织研究表明，经过 B_c 和 A 路径等径角挤压 4 道次后，出现了平均尺寸分别为 700 nm 和 1 μm 的细小晶粒，且大多数晶粒演化为大角度晶界排列。研究了铜管包覆对 7075 铝合金显微组织和织构的影响。

关键词：等径角挤压；晶体织构；铝合金；超细晶

(Edited by Xiang-qun LI)